

A semiclassical study of the topological Bose-Hubbard model

S. A. Owerre^{1,2,*}

¹*African Institute for Mathematical Sciences, 6 Melrose Road, Muizenberg, Cape Town 7945, South Africa.*

²*Perimeter Institute for Theoretical Physics, 31 Caroline St. N., Waterloo, Ontario N2L 2Y5, Canada.*

We present a semiclassical perspective of the topological Bose-Hubbard model recently studied by quantum Monte Carlo (QMC) simulation on the honeycomb lattice [Phys. Rev. B 93, 121401(R) (2016)]. The three insulating phases uncovered by QMC are as follows: a superfluid, a Mott phase, and a charge-density-wave insulating phase. We show that this model maps to a spin-1/2 quantum XY model with competing magnetic fields on the two honeycomb sublattices. We give an explicit analytical origin of the quantum phase diagram using mean-field theory. Basically, the competition between the sublattice magnetic fields leads to three distinct phases uncovered by QMC. We find that the mean-field phase diagram captures a large regime of the quantum phase diagram. Furthermore, due to the mapping from bosons to spin variables and vice versa, the bosonic excitations of the Bose-Hubbard model correspond to the magnon excitations of the quantum spin system. We corroborate this assertion by computing the magnon bulk bands and the Berry curvatures and we find that the Berry curvatures have the same trends as the QMC result.

PACS numbers: 75.10.Jm, 05.30.Jp, 37.10.Jk

Introduction–. We are used to the topological properties of fermion band theory in electronic systems, which have been studied extensively over the past decade.^{1–12} Recently, the idea of topological band theory has been extended to bosonic systems.^{13–27} However, in bosonic systems, there is no Fermi energy and the idea of completely filled band does not apply. This means that the topological invariant quantity usually called the Chern number must be independent of the statistical nature of the particles. It simply predicts the existence of edge state modes in the vicinity of the bulk energy gap as a result of the bulk-edge correspondence. This leads to edge states in bosonic systems.

An interesting feature of bosonic systems is that they can be mapped to spin-1/2 quantum magnets in the hard-core limit.²⁸ This correspondence is very crucial as it paves the way to interpret results in terms of bosons as well as spin variables. It also means that the excitations of hard-core bosons must be the underlying spin wave excitations (magnons) of the corresponding quantum spin model. Therefore, the topological properties of the bosonic excitations must be similar to that of spin wave excitations.²⁷ Unfortunately, many topological bosonic models have a numerical sign problem that hinders an explicit quantum Monte Carlo (QMC) simulation. In a recent study, Guo *et al*²³ have investigated the Bose-Hubbard model on the honeycomb lattice using QMC. This model is devoid of the debilitating QMC sign problem. They have explicitly mapped out the quantum phase diagram and the Berry curvature characterizing the topological properties of the system induced by a staggered on-site potential at the boundary.

In this paper, we present another perspective of their QMC results using a semiclassical approach. The results presented in Ref. [23] utilized the electronic analogue of the Bose-Hubbard model. Here, we show that this is not necessary. In fact, the entire QMC analysis can be understood semi-classically. This is due to the

fact that the extended Bose-Hubbard model is merely a spin-1/2 quantum XY model with competing sublattice magnetic fields, thus the results can also be interpreted in terms of magnetic spins and the semiclassical approach is known to be suitable for such models.^{29,30} We find that the quantum phase diagram uncovered by QMC can actually be understood by mean-field theory. We uncover the same three insulating phases: superfluid (SF), Mott insulator phase, and charge-density-wave (CDW) insulator. The latter insulating phase is a consequence of the competing sublattice magnetic fields. As mentioned above, the correspondence between hard-core bosons and quantum spin systems suggests that the spin wave excitations correspond to the bosonic excitations. Besides, the corresponding spin wave Hamiltonian is analogous to electronic graphene model with a staggered potential, hence the same analysis in electronic systems can be implemented directly. The topological properties of this system is manifested by a nonzero Berry curvature. We show that the Berry curvature (edge states) of the magnon excitations in the $\rho = 1/2$ CDW insulator has the same trend as the one obtain by QMC simulation.²³ These results have a great impact on the study of spin excitations in quantum magnetism.

Bose-Hubbard model–. A recent QMC simulation by Guo *et al*²³ studied the topological properties of the extended Bose-Hubbard model governed by the Hamiltonian

$$H = -t \sum_{\langle ij \rangle} (b_i^\dagger b_j + h.c.) + \sum_i U_i n_i - \mu \sum_i n_i, \quad (1)$$

where, $t > 0$ denotes NN hopping, μ is the chemical potential, and U_i is a staggered on-site potential; $n_i = b_i^\dagger b_i$, b_i^\dagger and b_i are the bosonic creation and annihilation operators respectively. They obey the algebra $[b_i, b_j^\dagger] = 0$ for $i \neq j$ and $\{b_i, b_i^\dagger\} = 1$. The Bose-Hubbard Hamiltonian (1) is simply a hard-core boson model, thus maps to a

spin-1/2 quantum XY model via the Matsubara-Matsuda transformation,²⁸ $S_i^+ \rightarrow b_i^\dagger$, $S_i^- \rightarrow b_i$, $S_i^z \rightarrow n_i - 1/2$. The resulting quantum spin Hamiltonian is given by

$$H = -J \sum_{\langle ij \rangle} (S_i^+ S_j^- + S_i^- S_j^+) - \sum_i (\mu - U_i) S_i^z, \quad (2)$$

where $S_i^\pm = S_i^x \pm iS_i^y$, while $U_i = \Delta$ on sublattice A , and $U_i = -\Delta$ on sublattice B . Thus, the last term is basically a competing magnetic field on the two sublattices. Throughout the analysis in this paper we fix $J = 0.5$, which corresponds to $t = 1$ in the hard-core bosons.

Mean-field phase diagram-. In this section, we present one of the main results of this paper — the mean-field phase diagram of the Bose-Hubbard model (1). The mean-field approximation is implemented by approximating the spins as classical vectors parameterized by a unit vector: $\mathbf{S}_i = S (\sin \theta_i \cos \phi_i, \sin \theta_i \sin \phi_i, \cos \theta_i)$. We adopt the customary two-sublattice honeycomb lattice depicted in Fig. (1). Since the spins lie on the same plane we take $\phi_i = 0$, then the classical energy is parameterized by θ_i given by

$$e_c = -\Delta_c \sin \theta_A \sin \theta_B - (\mu - \Delta) \cos \theta_A - (\mu + \Delta) \cos \theta_B, \quad (3)$$

where $e_c = E_c/Ns$, $\Delta_c = 2JzS$, $S = 1/2$, N is the

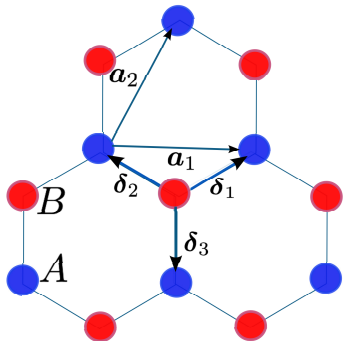


FIG. 1: Color online. The honeycomb lattice with two sublattices A and B indicated by different colors. The coordinates are $\mathbf{a}_1 = \sqrt{3}a\hat{x}$; $\mathbf{a}_{2,3} = a(-\sqrt{3}\hat{x}, \pm 3\hat{y})/2$; $\delta_{1,2} = a(\pm\sqrt{3}\hat{x}, \hat{y})/2$, and $\delta_3 = a(0, -\hat{y})$.

number of unit cells, and $z = 3$ is the coordination number of the lattice. The filling factor is given by $\rho = 1/2 + S(\cos \theta_A + \cos \theta_B)/2$.

There are three phases in this model uncovered by QMC.²³ In the mean-field approximation they are characterized by the polar angles. In the SF phase $\theta_A = \theta_B \neq 0, \pi$, the Mott phase is characterized by $\theta_A = \theta_B = 0$ or π , and the CDW is characterized by $\theta_A = 0$; $\theta_B = \pi$ or $\theta_A = \pi$; $\theta_B = 0$. The mean field phase diagram is derived by minimizing (3) following the standard approach.³¹ We obtain the phase boundary between SF and Mott insulators as $\mu_{c1} = \pm\sqrt{\Delta^2 + \Delta_c^2}$, whereas the phase boundary between SF and CDW insulators is $\mu_{c2} = \pm\sqrt{\Delta^2 - \Delta_c^2}$.

The classical angles are obtained explicitly as

$$\cos^2 \theta_A = \left(\frac{\Delta - \mu}{\Delta_c} \right)^2 \left[\frac{(\Delta + \mu)^2 + \Delta_c^2}{(\Delta - \mu)^2 + \Delta_c^2} \right], \quad (4)$$

$$\cos^2 \theta_B = \left(\frac{\Delta + \mu}{\Delta_c} \right)^2 \left[\frac{(\Delta - \mu)^2 + \Delta_c^2}{(\Delta + \mu)^2 + \Delta_c^2} \right]. \quad (5)$$

The mean-field phase diagram is depicted in Fig. (2). The superfluid phase appears for small μ , whereas the Mott phase is predominant for large μ . The CDW arises mainly from the competition between μ and Δ . The threshold limit Δ_c corresponds to the point where $\mu_{c2} = 0$. This is the exact same quantum phase diagram uncovered by QMC.²³

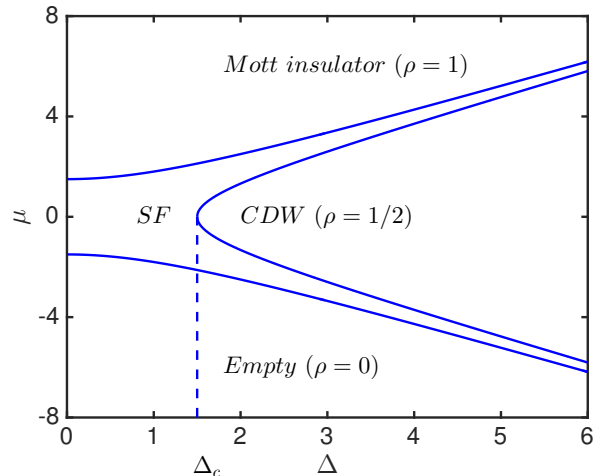


FIG. 2: Color online. Mean-field phase diagram of the Bose-Hubbard model (1), where $J = 0.5$ is the parameter value in the spin language, which corresponds to $t = 1$ in the hard-core bosons. The dash line indicates the critical value of the CDW phase.

Spin wave excitations-. The Bose-Hubbard model (1) describes an ordered system as shown in the phase diagram Fig. (2). In the spin language, we can study the excitations of the spin waves when quantum fluctuations are introduced and this will correspond to the excitations of the bosons. The simplest way to study spin wave excitations is via the standard Holstein Primakoff transformation. This approach is well-known to be sufficient for studying the ground state properties of hard-core bosons on two-dimensional lattices.^{29,30} In term of topological properties of quantum magnets, the Holstein Primakoff transformation has also been utilized effectively in this regard,^{14,15,17-19,26,27} and considered to be a good experimental predictor.²¹ In this section we utilize this semiclassical formalism in the study of the Bose-Hubbard model. The starting point of spin wave expansion is the rotation of the coordinate axes such that the z -axis coincides with the local direction of the classical polarization. This is implemented by a rotation about the y -axis on the

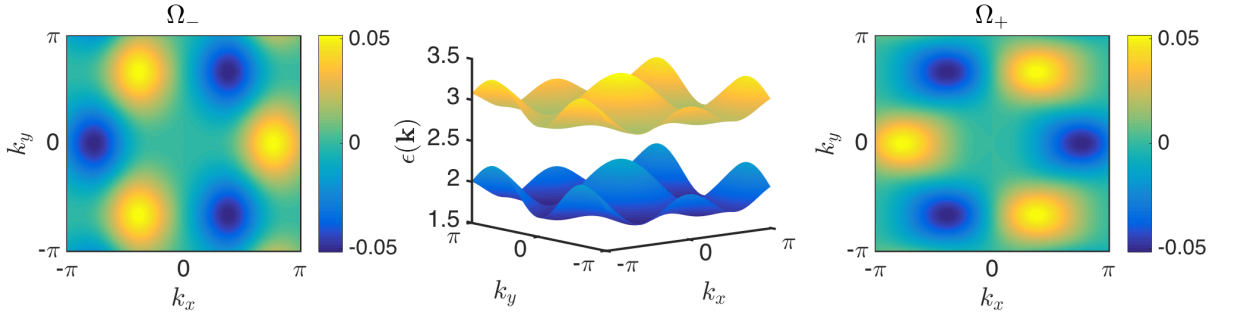


FIG. 3: Color online. Berry curvatures and the magnon bulk bands of the Bose-Hubbard model at $J = 0.5$, $\mu = 2J$, $\Delta = 4J$. This corresponds to the $\rho = 1/2$ CDW insulator in Fig. (2). The equal and opposite maximum peaks of the Berry curvatures are consistent with QMC simulation.²³

two sublattices

$$\begin{aligned} S_{i\alpha}^x &= S_{i\alpha}^{\prime x} \cos \theta_\alpha + S_{i\alpha}^{\prime z} \sin \theta_\alpha, \\ S_{i\alpha}^y &= S_{i\alpha}^{\prime y}, \\ S_{i\alpha}^z &= -S_{i\alpha}^{\prime x} \sin \theta_\alpha + S_{i\alpha}^{\prime z} \cos \theta_\alpha, \end{aligned} \quad (6)$$

where $\alpha = A, B$ label the sublattices.

We then introduce the linearized Holstein Primakoff transformation, $S_{i\alpha}^{\prime z} = S - c_{i\alpha}^\dagger c_{i\alpha}$, $S_{i\alpha}^{\prime y} = i\sqrt{S/2}(c_{i\alpha}^\dagger - c_{i\alpha})$, $S_{i\alpha}^{\prime x} = \sqrt{S/2}(c_{i\alpha}^\dagger + c_{i\alpha})$. The bosonic spin wave Hamiltonian becomes

$$\begin{aligned} H &= - \sum_{\langle ij \rangle} [v_1(c_{iA}^\dagger c_{jB} + h.c.) + v_2(c_{iA}^\dagger c_{jB}^\dagger + h.c.)] \\ &+ (v_A - m_A) \sum_i c_{iA}^\dagger c_{iA} + (v_B + m_B) \sum_j c_{jB}^\dagger c_{jB}, \end{aligned} \quad (7)$$

where $v_{1,2} = JS(\cos \theta_A \cos \theta_B \pm 1)$, $v_{A/B} = \Delta_c \sin \theta_A \sin \theta_B + \mu \cos \theta_{A/B}$ and $m_{A/B} = \Delta \cos \theta_{A/B}$. Apart from the off-diagonal terms with coefficient v_2 , Eq. (7) is similar to a graphene model with a staggered potential. In momentum space, we introduce the Nambu operators $\Psi_{\mathbf{k}}^\dagger = (\psi_{\mathbf{k}}^\dagger, \psi_{-\mathbf{k}})$, with $\psi_{\mathbf{k}}^\dagger = (c_{\mathbf{k}A}^\dagger, c_{\mathbf{k}B}^\dagger)$ and write Eq. (7) as

$$H = \frac{1}{2} \sum_{\mathbf{k}} \Psi_{\mathbf{k}}^\dagger \cdot \mathcal{H}(\mathbf{k}) \cdot \Psi_{\mathbf{k}} + \text{const.}, \quad (8)$$

$$\begin{aligned} \mathcal{H}(\mathbf{k}) &= \sigma_0[(v_A - m_A)\tau_+^0 + (v_B + m_B)\tau_-^0] \\ &- \tilde{v}_1 \sigma_0(\tau_+ \gamma_{\mathbf{k}} + h.c.) - \tilde{v}_2 \sigma_x(\tau_+ \gamma_{\mathbf{k}} + h.c.) \end{aligned} \quad (9)$$

where $\tilde{v}_{1,2} = zv_{1,2}$. We have introduced two Pauli matrices $\boldsymbol{\sigma}$ and $\boldsymbol{\tau}$, where $\tau_\pm = (\tau_x \pm i\tau_y)/2$, while σ_0 is an identity 2×2 matrix in the $\boldsymbol{\sigma}$ -space. We also introduce other matrices for simplification, $\tau_+^0 = \text{diag}(1, 0)$, $\tau_-^0 = \text{diag}(0, 1)$. The structure factor is $\gamma_{\mathbf{k}} = \frac{1}{z} \sum_\mu e^{i\mathbf{k} \cdot \boldsymbol{\delta}_\mu}$ where $\boldsymbol{\delta}_\mu$ are the NN vectors shown in Fig. (1). The spin wave Hamiltonian (8) is Hermitian but it is not diagonal. To diagonalize this Hamiltonian, we make a transformation $\Psi_{\mathbf{k}}^\dagger \rightarrow \mathcal{U}(\mathbf{k})\tilde{\Psi}_{\mathbf{k}}^\dagger$, which satisfies the relation

$$\mathcal{U}^\dagger \mathcal{H}(\mathbf{k}) \mathcal{U} = \epsilon(\mathbf{k}); \quad \mathcal{U}^\dagger \eta \mathcal{U} = \eta, \quad (10)$$

with $\eta = \sigma_z \mathbf{I}_\tau$. The matrix $\tilde{\Psi}_{\mathbf{k}}^\dagger$ contains the Bogoliubov operators $(\alpha_{\mathbf{k}}^\dagger, \beta_{\mathbf{k}}^\dagger)$ and $\epsilon(\mathbf{k}) = [\epsilon(\mathbf{k}), -\epsilon(\mathbf{k})]$ are the eigenvalues. This transformation leads to a non-Hermitian Bogoliubov Hamiltonian $\mathcal{H}_B(\mathbf{k}) = \eta \mathcal{H}(\mathbf{k})$, which is given by

$$\begin{aligned} \mathcal{H}_B(\mathbf{k}) &= \sigma_z[(v_A - m_A)\tau_+^0 + (v_B + m_B)\tau_-^0] \\ &- \tilde{v}_1 \sigma_z(\tau_+ \gamma_{\mathbf{k}} + h.c.) - \tilde{v}_2 i \sigma_y(\tau_+ \gamma_{\mathbf{k}} + h.c.). \end{aligned} \quad (11)$$

Magnon bands and Berry Curvatures- To study the topological properties of this model we need to diagonalize Eq. (11), whose eigenvalues give the magnon energy bulk bands. The Hamiltonian can be diagonalized, but the eigenvalues are too long to write here. Due to the $-\mathbf{k}$ quasiparticles, there are two positives and two negatives magnon bands; we consider only the positive eigenvalues. For $\Delta = 0$, we have $m_A = m_B = 0$, then Eqs. (4) and (5) simply give $\theta_A = \theta_B = \theta$, hence $v_A = v_B$ and Eq. (11) reduces to the usual hard-core bosons or XY model. In this limit, there are no topological effects in the magnon bulk bands, but the system exhibits Dirac nodes at $\mathbf{K}(\mathbf{K}') = (\pm 4\pi/3\sqrt{3}a, 0)$ and a Goldstone mode at $\mathbf{k} = 0$. As QMC demonstrated,²³ the topological properties of this system is induced by a nonzero Δ which implies that $m_A \neq 0$ and $m_B \neq 0$.

Due to a non-vanishing mass, there is a Berry curvature associated with the magnon bulk gap. It is given by

$$\Omega_\lambda(\mathbf{k}) = - \sum_{\lambda \neq \lambda'} \frac{2\text{Im}[\langle \psi_{\mathbf{k}\lambda} | v_x | \psi_{\mathbf{k}\lambda'} \rangle \langle \psi_{\mathbf{k}\lambda'} | v_y | \psi_{\mathbf{k}\lambda} \rangle]}{(\epsilon_{\mathbf{k}\lambda} - \epsilon_{\mathbf{k}\lambda'})^2}, \quad (12)$$

where $v_i = \partial \mathcal{H}_B(\mathbf{k}) / \partial k_i$ defines the velocity operators and $\lambda = \pm$ denotes the two positive magnon bands. The CDW insulator is the nontrivial phase in this model, we will focus on this insulator. Figure (3) shows the magnon energy bands and the corresponding Berry curvatures for the top and the bottom bands in the $\rho = 1/2$ CDW insulator. The Berry curvatures show equal and opposite maximum peaks at the corners of the Brillouin zone. This is in good agreement with QMC simulation.²³ Notice that the sum of the two Berry curvatures vanishes, this implies that no edge states exist above the upper band.^{23,27}

In addition, we have shown the structure of the $\rho = 1/2$ CDW dispersion. The existence of edge states is already encoded in the nonzero Berry curvature. They can be determined in the usual way as we have previously shown with a model in which QMC has a sign problem.²⁷ Although, the mass term in the present model is momentum independent, the idea is essentially the same. From the magnon Hamiltonian (7), it is evident that the magnon model is analogous to that of graphene, so one could follow a similar procedure as demonstrated in Ref. [11,12] to solve for the edge states and a similar situation still emerge.

Conclusion–. The main result of this paper is that the topological properties of hard-core bosons correspond to the nontrivial topological properties of the magnon excitations of the corresponding quantum spin model. We have shown an example of this assertion using the extended Bose-Hubbard model recently studied by quantum Monte Carlo (QMC) simulation.²³ In this model,

competing sublattice magnetic fields lead to a nontrivial charge-density-wave insulator with a filling factor of $\rho = 1/2$, in addition to superfluid and Mott insulators. We have uncovered the mean-field phase diagram, which is shown to be consistent with the QMC phase diagram. We also derived the magnon energy bands of the insulators and show that the corresponding Berry curvatures (edge states) are consistent with QMC simulations. The result derived in this paper is important as it opens a wide spectrum of theoretical and experimental research in magnon excitations of quantum magnetic systems. This basic idea we have presented here can also be generalized to bilayer honeycomb lattice and other systems.

Acknowledgments–. The author would like to thank African Institute for Mathematical Sciences (AIMS). Research at Perimeter Institute is supported by the Government of Canada through Industry Canada and by the Province of Ontario through the Ministry of Research and Innovation.

* Electronic address: solomon@aims.ac.za

- ¹ M. Z. Hasan and C. L. Kane, Rev. Mod. Phys. **82**, 3045 (2010).
- ² X.-L. Qi and S.-C. Zhang, Rev. Mod. Phys. **83**, 1057 (2011).
- ³ R. Yu *et al.*, Science, **329**, 61 (2010).
- ⁴ Y. L. Chen *et al.*, Science **329**, 659 (2010).
- ⁵ C.L. Kane and E.J. Mele, Phys. Rev. Lett. **95**, 146802 (2005); *ibid* Phys. Rev. Lett. **95**, 226801 (2005) .
- ⁶ J.E. Moore and L. Balents, Phys. Rev. B **75**, 121306 (2007).
- ⁷ L. Fu, C.L. Kane, and E.J. Mele, Phys. Rev. Lett. **98**, 106803 (2007).
- ⁸ D. Hsieh *et al.*, Nature **452**, 970 (2008).
- ⁹ H. Zhang *et al.*, Nature Phys. **5**, 438, (2009).
- ¹⁰ F. D. M. Haldane, Phys. Rev. B **61**, 2015 (1988).
- ¹¹ G. W. Semenoff, V. Semenoff, and F. Zhou, Phys. Rev. Lett. **101**, 087204 (2008).
- ¹² W. Yao, S. A. Yang, and Q. Niu, Phys. Rev. Lett. **102**, 096801 (2009).
- ¹³ C. N. Varney *et al.*, Phys. Rev. B **82**, 115125 (2010).
- ¹⁴ H. Katsura, N. Nagaosa, and P. A. Lee, Phys. Rev. Lett. **104**, 066403 (2010).
- ¹⁵ S. Y. Onose *et al.*, Science **329**, 297 (2010).

- ¹⁶ Y. F. Wang *et al.*, Phys. Rev. Lett. , **107**, 146803 (2011).
- ¹⁷ R. Matsumoto and S. Murakami, Phys. Rev. Lett. **106**, 197202 (2011); Phys. Rev. B **84**, 184406 (2011).
- ¹⁸ A. Mook, J. Henk, and I. Mertig, Phys. Rev. B **90**, 024412 (2014); Phys. Rev. B **89**, 134409 (2014).
- ¹⁹ H. Lee, J. H. Han, and P. A. Lee, Phys. Rev. Lett. **91**, 125413 (2015).
- ²⁰ R. Chisnell *et al.*, Phys. Rev. Lett. **115**, 147201 (2015).
- ²¹ M. Hirschberger *et al.*, Phys. Rev. Lett. **115**, 106603 (2015).
- ²² I. Vasić *et al.*, Phys. Rev. B **91**, 094502 (2015).
- ²³ H. Guo *et al.*, Phys. Rev. B **93**, 121401(R) (2016).
- ²⁴ F. -Y. Li *et al.*, arXiv:1602.04288.
- ²⁵ S. A. Owerre, arXiv:1602.06772.
- ²⁶ S. A. Owerre, arXiv:1603.04331.
- ²⁷ S. A. Owerre, arXiv:1603.06495.
- ²⁸ T. Matsubara and H. Matsuda, Prog. Theor. Phys. **16**, 569 (1956).
- ²⁹ K. Bernardet *et al.*, Phys. Rev. B **65**, 104519 (2002).
- ³⁰ T. Coletta, N. Laflorencie, and F. Mila, Phys. Rev. B **85**, 104421 (2012).
- ³¹ G. Murthy, D. Arovas, and A. Auerbach, Phys. Rev. B **55**, 3104 (1997).